Guiding light via geometric phases: Supplementary Materials

(Dated: March 11, 2016)

We derive the model equations introduced in the main text and present numerical (FDTD) simulations in support of the most relevant results. We also discuss a few additional features.

I. LIGHT PROPAGATION IN A PERIODIC SYSTEM ENCOMPASSING A ROTATION OF THE OPTIC AXIS IN THE TRANSVERSE PLANE

We consider light propagation in inhomogeneous anisotropic dielectrics, in particular uniaxials; nonetheless, our results can be readily generalized to biaxial crystals. We take a medium whose dielectric properties vary across the transverse coordinate x owing exclusively to a rotation of the optic axis in the plane xy orthogonal to the propagation coordinate z. We consider finite wavepackets with wavevector parallel to $\hat{z}$; hence, corresponding to electric fields oscillating orthogonally and parallel to the optic axis, respectively, the two independent eigenvalues $\epsilon_\perp$ and $\epsilon_\parallel$ of the relative permittivity tensor are constant in space. We define the birefringence $\Delta n = \sqrt{\epsilon_\parallel} - \sqrt{\epsilon_\perp} = n_e - n_o$ and assume that the distribution of the optic axis is purely planar and transverse to $\hat{z}$, such that at each z the rotation can be described by a standard 2D operator acting in xy:

$$\boldsymbol{R}_{xy}(\theta) = \begin{pmatrix} \cos\theta & \sin\theta \\ -\sin\theta & \cos\theta \end{pmatrix}, \tag{S1}$$

where the angle θ is defined with respect to the y axis of a Cartesian reference system in the laboratory frame, with $\theta = 0$ corresponding to a dielectric permittivity $\epsilon_\parallel$ for electric fields along y. We study forward propagating light waves in the presence of a periodic modulation of θ along z. To this extent we set

$$\theta(x,z) = \sigma(z)\Gamma(x) = \left(\sum_{p=-\infty}^{\infty} \sigma_p e^{\frac{i2\pi pz}{\Lambda}} \right) \Gamma(x), \tag{S2}$$

with $\sigma(z)$ a function periodic with Λ and $\Gamma(x)$ the transverse distribution of optic axis orientation, the latter being uniform across y. Hereafter, we focus on the case of a purely sinusoidal modulation $\sigma_p = \sigma_1\delta_{1,p} + \sigma_{-1}\delta_{-1,p}$, with $\delta_{p,p'}$ the Kronecker's delta and $\sigma_{-1} = \sigma_1^*$ in order for σ to be real valued. For the sake of simplicity, we refer to positive uniaxial media with $\Delta n > 0$: the generalization to negative birefringence is straightforward. Moreover, we deal with the case $\Lambda = \lambda/\Delta n$ in which resonant effects are expected to occur.

In the paraxial limit (neglecting longitudinal field components) and for small birefringence ($\Delta n \ll 1$), Maxwell equations in two dimensions (i.e., no field evolution across y) can be cast as

$$\frac{\partial^2}{\partial z^2}\begin{pmatrix} E_x \\ E_y \end{pmatrix} = -\frac{\partial^2}{\partial x^2}\begin{pmatrix} E_x \\ E_y \end{pmatrix} - k_0^2 \begin{pmatrix} \epsilon_{xx}(x,z) & \epsilon_{xy}(x,z) \\ \epsilon_{yx}(x,z) & \epsilon_{yy}(x,z) \end{pmatrix} \begin{pmatrix} E_x \\ E_y \end{pmatrix}, \tag{S3}$$

where $\boldsymbol{\psi}_{xy} = (E_x; E_y)$ is the two-component Jones vector representing the electric field in the complex notation.

In order to investigate the propagation of an electromagnetic (optical) wave in such a system, we make use of the transformation $\boldsymbol{\psi}_{oe} = \boldsymbol{R}_{xy} \cdot \boldsymbol{\psi}_{xy}$ and write $\boldsymbol{\psi}_{oe} = (E_o; E_e)$, with E_o and E_e the pointwise ordinary and extraordinary polarization components of the electric field, respectively. In the rotated reference system the two-dimensional dielectric tensor is diagonal, specifically $\boldsymbol{\epsilon}_D = (\epsilon_\perp, 0; 0, \epsilon_\parallel)$. Eq. (S3) then becomes

$$\begin{aligned} &\frac{\partial^2 \boldsymbol{\psi}_{oe}}{\partial z^2} - 2i\frac{\partial\theta}{\partial z}\boldsymbol{S}_2 \cdot \frac{\partial \boldsymbol{\psi}_{oe}}{\partial z} = -\frac{\partial^2 \boldsymbol{\psi}_{oe}}{\partial x^2} + 2i\frac{\partial\theta}{\partial x}\boldsymbol{S}_2 \cdot \frac{\partial \boldsymbol{\psi}_{oe}}{\partial x} + i\left(\frac{\partial^2\theta}{\partial x^2} + \frac{\partial^2\theta}{\partial z^2}\right)\boldsymbol{S}_2 \cdot \boldsymbol{\psi}_{oe} \\ &+ \left[\left(\frac{\partial\theta}{\partial x}\right)^2 + \left(\frac{\partial\theta}{\partial z}\right)^2\right]\boldsymbol{\psi}_{oe} - k_0^2 \boldsymbol{\epsilon}_D \cdot \boldsymbol{\psi}_{oe}, \end{aligned} \tag{S4}$$

where we introduced the Pauli matrix $\boldsymbol{S}_2 = (0, -i; i, 0)$. Equation (S4) shows that a scalar potential proportional to $(\partial\theta/\partial x)^2 + (\partial\theta/\partial z)^2$ acts on both field components. Additionally, other terms (containing the matrix $\boldsymbol{S}_2$) couple ordinary and extraordinary polarizations: due to the rotation of the optic axis, the ordinary and extraordinary components are no longer independent, but can affect each other during propagation.

In the slowly varying envelope approximation (SVEA), we first set $E_o = \psi_o(x,z)e^{ik_0 n_o z}$ and $E_e = \psi_e(x,z)e^{ik_0 n_e z}$ in Eq. (S4). Exploiting the system periodicity in z we then introduce the following further transformation:

$$\psi_j(x,z) = A_j(x,z)B_j(x,z) \quad (j = e, o), \tag{S5}$$

where $A_j(x,z)$ are the slow-varying envelopes for the two wave components and $B_j(x,z)$ are periodic functions of z accounting for the effect of the medium modulations with period Λ. It is convenient to write the latter ones in an exponential form as follows:

$$B_j(x,z) = e^{i\left[\int \sum_{\substack{p=-\infty \\ p\neq 0}}^{\infty} \beta_p^{(j)}(x,z)dz\right]} = \exp\left[\sum_{\substack{p=-\infty \\ p\neq 0}}^{\infty} \frac{\Lambda}{2\pi p}\beta_p^{(j)}(x)e^{\frac{i2\pi pz}{\Lambda}}\right] \tag{S6}$$

where we set $\beta_p^{(j)}(x,z) = \beta_p^{(j)}(x)e^{\frac{i2\pi pz}{\Lambda}}$ and the constant term $p=0$ must be excluded from the sum. Inserting these ansätze in Eq. (S4) and expanding in powers of Λ all terms one obtains a hierarchy of coupled equations for the amplitudes $A_j(x,z)$ and the coefficients $\beta_p^{(j)}(x)$. Neglecting from these equations all terms with powers of the period Λ equal to or larger than 1 and higher-order terms in λ/Λ (which is equal to Δn at resonance), we obtain the following coupled equations for the slow amplitudes:

$$i\frac{\partial A_o}{\partial z} = -\frac{1}{2\bar{n}k_0}\frac{\partial^2 A_o}{\partial x^2} + \frac{1}{2\bar{n}k_0}\left[\overline{\sigma^2(z)}\left(\frac{d\Gamma}{dx}\right)^2 + \Gamma^2\overline{\left(\frac{d\sigma}{dz}\right)^2}\right]A_o + \frac{2\pi}{\Lambda}\sigma_{-1}\Gamma(x)A_e, \tag{S7}$$

$$i\frac{\partial A_e}{\partial z} = -\frac{1}{2\bar{n}k_0}\frac{\partial^2 A_e}{\partial x^2} + \frac{1}{2\bar{n}k_0}\left[\overline{\sigma^2(z)}\left(\frac{d\Gamma}{dx}\right)^2 + \Gamma^2\overline{\left(\frac{d\sigma}{dz}\right)^2}\right]A_e + \frac{2\pi}{\Lambda}\sigma_{1}\Gamma(x)A_0, \tag{S8}$$

where $\overline{m(z)} = \frac{1}{\Lambda}\int_0^\Lambda m(z)dz$ and $\bar{n} = (n_e + n_o)/2$.

After inspection of Eqs. (S7-S8), three salient terms stand out:

- a Kapitza-like potential, proportional to the squared transverse derivative of the distribution Γ of optic axis orientation; its magnitude is modulated by the mean square of the periodic modulation $\sigma(z)$;
- an effective transverse potential with profile proportional to Γ^2; its magnitude is modulated by the mean square of the longitudinal derivative of the periodic modulation $\sigma(z)$;
- a phase-matched coupling between ordinary and extraordinary waves via the fundamental harmonics $\sigma_{\pm 1}$ of the periodic modulation.

The equations (S7-S8) can be recast in a more compact form as

$$i\frac{\partial \boldsymbol{A}}{\partial z} = \boldsymbol{L}_{\mathrm{ISO}}\cdot\boldsymbol{A} + \boldsymbol{L}_{\mathrm{ANI}}\cdot\boldsymbol{A}, \tag{S9}$$

where $\boldsymbol{A} = (A_o;\ A_e)$ and we introduced the isotropic (matrix) operator

$$\boldsymbol{L}_{\mathrm{ISO}} = \frac{1}{2\bar{n}k_0}\left\{-\frac{\partial^2}{\partial x^2} + \left[\overline{\sigma^2}\left(\frac{d\Gamma}{dx}\right)^2 + \Gamma^2\overline{\left(\frac{d\sigma}{dz}\right)^2}\right]\right\}\boldsymbol{I}, \tag{S10}$$

and the anisotropic operator

$$\boldsymbol{L}_{\mathrm{ANI}} = \frac{2\pi}{\Lambda}\Gamma(x)\begin{pmatrix} 0 & \sigma_{-1} \\ \sigma_1 & 0 \end{pmatrix}. \tag{S11}$$

The presence of $\boldsymbol{L}_{\mathrm{ANI}}$ in Eq. (S9) accounts for the power exchange between ordinary and extraordinary components.

Let us now take $\sigma(z) = \sin(\frac{2\pi z}{\Lambda})$, that is $\sigma_1 = -i/2$ and $\sigma_{-1} = i/2$; then $\boldsymbol{L}_{\mathrm{ANI}} = -\frac{\pi}{\Lambda}\Gamma(x)\boldsymbol{S}_2$. The eigenvalues of the Pauli matrix $\boldsymbol{S}_2$ are $s_z = \pm 1$ with the two circular polarizations $(1;\ \pm i)/\sqrt{2}$ for eigenvectors (plus and minus correspond to RCP and LCP in our convention, respectively). Therefore, when the optic axis is modulated along z with period equal to the beat length, the localized wave solutions are circularly polarized. By using the transformation

$$\boldsymbol{A}_{oe} = \boldsymbol{P}\cdot\boldsymbol{A}_{LR} = \frac{1}{\sqrt{2}}\begin{pmatrix} 1 & 1 \\ -i & i \end{pmatrix}\begin{pmatrix} A_L \\ A_R \end{pmatrix}, \tag{S12}$$

the system of equations separates into two independent scalar equations

$$i\frac{\partial A_L}{\partial z} = -\frac{1}{2\bar{n}k_0}\frac{\partial^2 A_L}{\partial x^2} + \frac{1}{4\bar{n}k_0}\left[\left(\frac{d\Gamma}{dx}\right)^2 + \frac{4\pi^2}{\Lambda^2}\Gamma^2(x)\right]A_L + \frac{\pi}{\Lambda}\Gamma(x)A_L, \tag{S13}$$

$$i\frac{\partial A_R}{\partial z} = -\frac{1}{2\bar{n}k_0}\frac{\partial^2 A_R}{\partial x^2} + \frac{1}{4\bar{n}k_0}\left[\left(\frac{d\Gamma}{dx}\right)^2 + \frac{4\pi^2}{\Lambda^2}\Gamma^2(x)\right]A_R - \frac{\pi}{\Lambda}\Gamma(x)A_R, \tag{S14}$$

where we used $\overline{\sigma^2(z)} = 0.5$ and $\overline{(d\sigma/dz)^2} = 2\pi^2/\Lambda^2$. The guided eigenmodes are then defined by setting $A_i(x,z) = e^{i\beta_0 z}A_i(x,0)$, where β_0 is the propagation constant. The problem is then transformed into a standard eigenvalue problem, with the following equations:

$$-2k_0\bar{n}\beta_0 A_L = -\frac{\partial^2 A_L}{\partial x^2} + \left[\frac{1}{2}\left(\frac{d\Gamma}{dx}\right)^2 + \frac{2\pi^2}{\Lambda^2}\Gamma^2(x)\right]A_L + \frac{2k_0\bar{n}\pi}{\Lambda}\Gamma(x)A_L, \tag{S15}$$

$$-2k_0\bar{n}\beta_0 A_R = -\frac{\partial^2 A_R}{\partial x^2} + \left[\frac{1}{2}\left(\frac{d\Gamma}{dx}\right)^2 + \frac{2\pi^2}{\Lambda^2}\Gamma^2(x)\right]A_R - \frac{2k_0\bar{n}\pi}{\Lambda}\Gamma(x)A_R, \tag{S16}$$

Equations (S15) and (S16) are valid for left (LCP) and right (RCP) circularly polarized wavepackets at the input interface, respectively. It is noteworthy that RCP and LCP interchange roles if the modulation $\sigma(z)$ is shifted by half a period, in agreement with the intuitive picture provided in the main text.

A. Polarization-dependent effective index well

In standard (1+1)D graded-index waveguides, a generic transverse-electric mode u satisfies $-2k_0\bar{n}\kappa u = -\frac{\partial^2 u}{\partial x^2} - k_0^2\Delta n^2 u$, with κ the propagation constant. Thus, from Eqs. (S15-S16) it is apparent that the two circular polarizations perceive the effective photonic potential $V_{\text{eff}} = -k_0\Delta n^2_{\text{eff}}/(2\bar{n})$ with the index distributions $\Delta n^2_{\text{eff}}(x)$ given by

$$\Delta n^2_{\text{eff},LCP} = -\frac{2\bar{n}}{k_0}V_{\text{eff},LCP} = -\frac{1}{k_0^2}\left[\frac{1}{2}\left(\frac{d\Gamma}{dx}\right)^2 + \frac{2\pi^2}{\Lambda^2}\Gamma^2(x)\right] + \bar{n}\frac{\lambda}{\Lambda}\Gamma(x), \tag{S17}$$

$$\Delta n^2_{\text{eff},RCP} = -\frac{2\bar{n}}{k_0}V_{\text{eff},RCP} = -\frac{1}{k_0^2}\left[\frac{1}{2}\left(\frac{d\Gamma}{dx}\right)^2 + \frac{2\pi^2}{\Lambda^2}\Gamma^2(x)\right] - \bar{n}\frac{\lambda}{\Lambda}\Gamma(x), \tag{S18}$$

The polarization independent term between square brackets in Eqs. (S17-S18) is a Kapitza-like equivalent photonic potential stemming from transverse and longitudinal modulation of the rotating optic axis. Since this photonic potential is independent from $k_0 = 2\pi/\lambda$, by itself it would support guided modes with wavelength-independent profile [1].

The last terms on the RHS of Eqs. (S17-S18), with opposite signs as wave handedness reverses, are responsible for the strong dependence of light evolution on input polarization: the periodic rotation of the optic axis along z allows for an *accumulation* of the Berry phase during propagation, leading to the appearance of a potential proportional to Γ. Moreover, since phase-matching requires $\Lambda = \lambda/\Delta n$, such potential is directly proportional to the medium birefringence. A quantitative study on the relevance of each term in Eqs. (S17-S18) is reported in the following section.

B. Bell-shaped orientation distribution of the optic axis

Hereafter we make explicit reference to optical frequencies. Nevertheless, since Maxwell equations are invariant when dividing all the length scales by a given factor and multiplying the frequency by the same factor, our results clearly hold valid regardless the electromagnetic band.

Supplementary Fig. 1 shows the effective index well $-\Delta n^2_{\text{eff}}$ (sign-inverted, so light is attracted by the dip) as computed from Eqs. (S17-S18) when the transverse distribution of the orientation angle $\Gamma(x)$ is bell-shaped and centered in $x = 0$. We assumed $\Gamma(x) = \Gamma_0 \exp(-x^2/w_D^2)$, with Γ_0 and w_D the maximum orientation angle and the width of the distribution, respectively. Using this simple ansatz we can address the role of each term in the effective index well, Eqs. (S17-S18). The term proportional to $(d\Gamma/dx)^2$ is a Kapitza-like term: when acting alone it yields

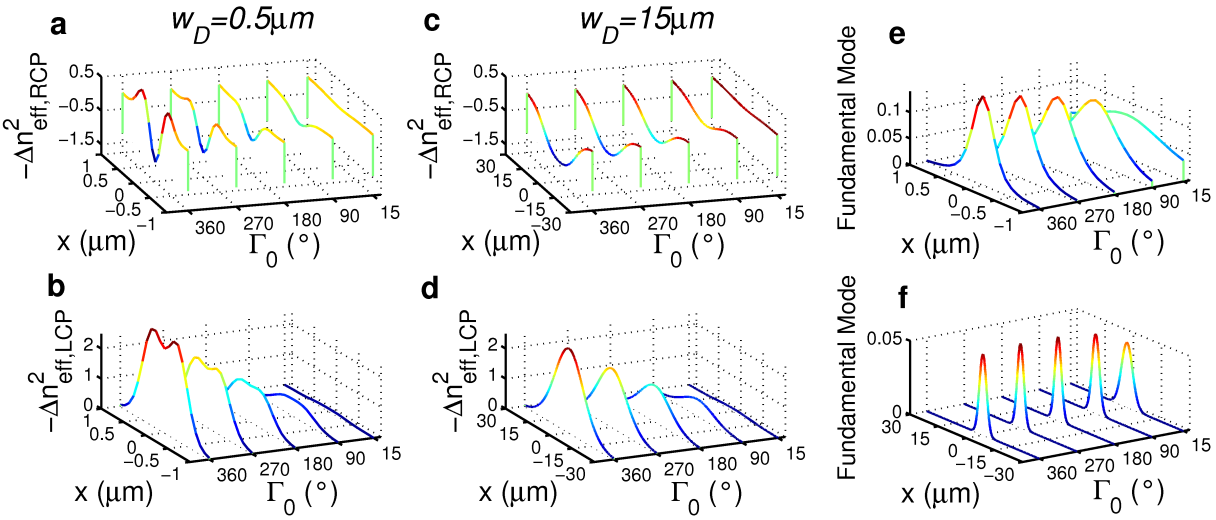

Supplementary Figure 1. **a-d** Transverse profile of the sign-inverted effective index distribution, proportional to the photonic potential $V_{\text{eff},LCP/RCP}$ versus maximum reorientation angle Γ_0 for two different widths (**a-b**) $w_D = 0.5$ μm and (**c-d**) $w_D = 15$ μm of the transverse angular distribution. Input RCP waves are trapped in **a, c** and input LCP waves undergo defocusing in **b, d**, respectively, in agreement with the chosen initial section. **e-f** Profiles of the fundamental guided (RCP) mode when (**e**) $w_D = 0.5$ μm and (**f**) $w_D = 15$ μm. Here $\lambda = 1$ μm, $n_o = 1.5$ and $n_e = 1.7$.

quasi-modes, as detailed in Ref. [2]. This contribution to the index landscape, proportional to w_D^{-2}, increases as the angle distribution becomes narrower. Supplementary Fig. 1 illustrates two examples for $w_D = 0.5$ μm and $w_D = 15$ μm, respectively: the Kapitza term becomes quite relevant for $w_D = 0.5$ μm and large Γ_0, with the appearance of two local maxima, symmetrically placed with respect to the axis $x = 0$. The term proportional to $\Gamma^2(x)$ gives rise to anti-guidance, i.e. light repulsion from the symmetry axis. The term is proportional to the square of the birefringence Δn, thus dominates for large anisotropies.

Finally, the last term breaks the degeneracy between the two opposite circular polarizations. This term contributes with opposite signs to the overall potential acting on RCP and LCP waves, respectively: in the absence of other contributions, when the RCP (LCP) wave is confined, the LCP (RCP) is repelled from the region close to the symmetry axis $x = 0$, i.e., it diffracts faster than in a homogeneous medium.

C. Finite-Difference-Time-Domain numerical simulations of the guiding case

In the numerical simulations we employed the open-source FDTD code named MEEP [3] to solve the full Maxwell equations in two dimensions, assuming a Gaussian orientation of the optic axis across x, as above. The excitation was a continuous-wave source of wavelength 1 μm turned on at $t = 0$, infinitely narrow across z and launched in $x = z = 0$. The source had a Gaussian profile of width 3 μm across x and was point-like along z. The modulated uniaxial medium was placed in $z > z_0 = 2$ μm with modulation $\sigma(z) = \sin\left[\frac{2\pi\Delta n}{\lambda}(z - z_0)\right]$. The refractive indices n_o and n_e were taken equal to 1.5 and 1.7, respectively.

Supplementary Fig. 2 illustrates the propagation of an RCP wave input when $w_D = 5$ μm and $\Gamma_0 = 15°$, corresponding to a guiding potential (see Fig. 2 in the main text). As predicted, the natural diffractive spreading is compensated for by the effective waveguide resulting from Berry phase accumulation. At distances far enough from the input, in the stationary regime, the wavepacket acquires a periodic spatial distribution of its polarization and a nearly invariant profile. The polarization is generally elliptical; its trend can be examined by taking a single period $\lambda/\Delta n$ far enough from the input so that radiation (from imperfect coupling) is negligible. The polarization at the input is RCP, then it starts decreasing ellipticity; at about a quarter period it becomes linear, then elliptical again but with opposite handedness; at half period is nearly LCP, in excellent agreement with the theory. In the following half-period the polarization evolves in a similar manner, going from LCP to RCP. The polarization rotation versus propagation strictly resembles the behavior of a plane wave because it originates from the different phase velocities of the two linear eigenfield carriers (with $e^{ik_0 n_o z}$ and $e^{ik_0 n_e z}$, respectively).

Supplementary Fig. 3 compares the intensity evolution of propagating LCP and RCP wavepackets. In agreement with theory, one input polarization is subject to trapping, the other to a repulsive potential expelling light from the

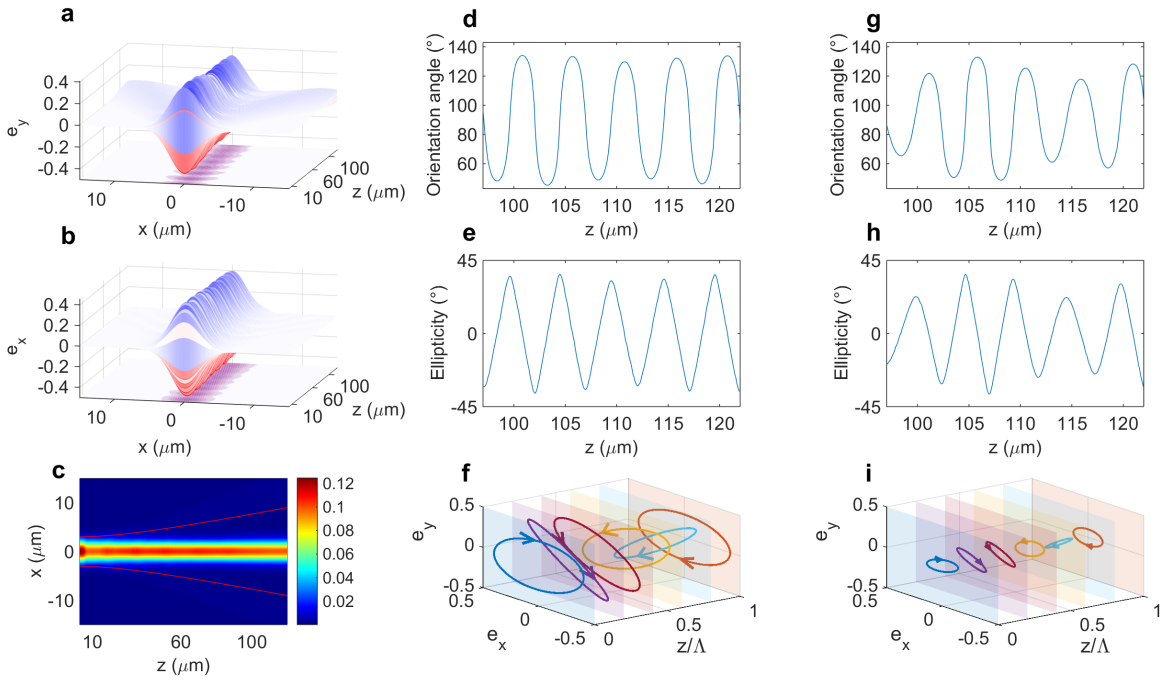

Supplementary Figure 2. Numerical snapshots of (**a**) e_y and (**b**) e_x in the plane xz once the stationary regime is reached in time; (**c**) corresponding average intensity map in xz; the red solid lines correspond to beam diffraction when $\Gamma_0 = 0$, i.e., the homogeneous case. (**d, g**) Angular orientation of the polarization ellipse and **e, h**) field ellipticity (arctangent of the ratio of minor to major axes) versus z in (**d-e**) $x = 0$ and (**g-h**) $x = 3$ μm, respectively . Polarization ellipses in (**f**) $x = 0$ and (**i**) $x = 3$ μm plotted versus z in an interval $0 \leq z\Delta n/\lambda \leq 1$ far away from the excitation point, corresponding to 97 μm$\leq z \leq$ 102 μm. Here $w_D = 5$ μm, $\Gamma_0 = 15°$, RCP input.

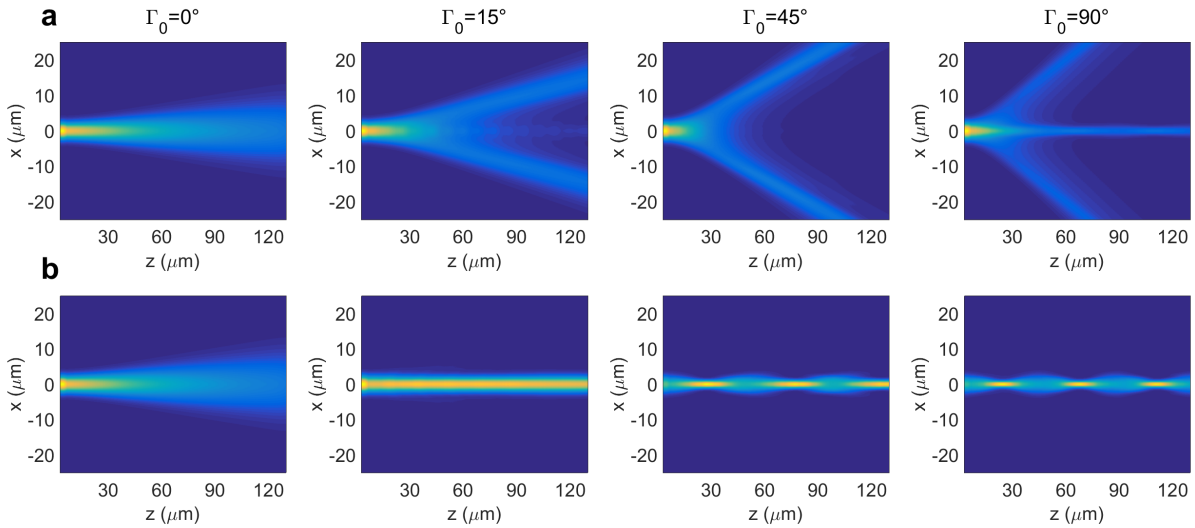

Supplementary Figure 3. Average beam intensity in the plane xz when the input is (**a**) LCP or (**b**) RCP. The maximum rotation Γ_0 is 0, 15, 45 and 90°, from left to right, respectively. Here $z_0 = 0$ and $w_D = 5$ μm.

region around $x = 0$. The strength of either potentials increases with the maximum rotation Γ_0: in the trapping case the waveguide eventually becomes multi-modal, as indicated by the appearance of breathing versus propagation; in the repulsive case the beam divergence increases with Γ_0. For $\Gamma_0 \geq 90°$ the polarization of the confined beam continues to oscillate along z, but in the presence of higher harmonics. In fact, in Eq. (S6) the functions $\beta_p(x, z)$ with $p \geq 1$ must be accounted for and correspond to shorter periodicity in both beam profile and polarization. Simultaneously,

a higher-order contribution proportional to $\Lambda^2(\frac{d\Gamma}{dx}\frac{d^2\Gamma}{dx^2})^2$ appears in the overall photonic potential of the isotropic operator $\boldsymbol{L}_{\mathrm{ISO}}$ defined by Eq. (S10) [4]. Accordingly, even in the defocusing case a small portion of the wavepacket is trapped on-axis around $x = 0$ for $\Gamma_0 = 90°$, as visible in Fig. 3. Owing to the additional modulating terms $\beta_p^{(j)}(x)$, further increases in Γ_0 (not shown) infringe the validity of Eqs. (S15-S16), leading to the generation of three-peaks for both input polarizations as well as appreciable changes of polarization state across x in the guided case.

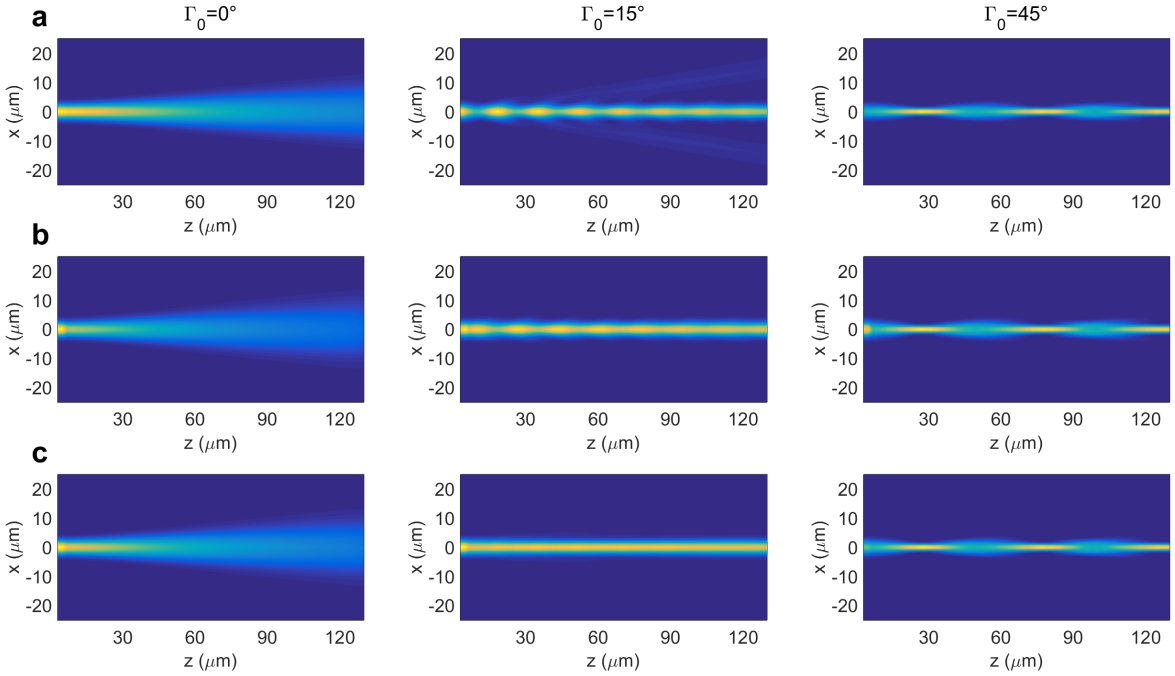

Supplementary Figure 4. Evolution maps of (**a**) $|E_y|^2$, (**b**) $|E_x|^2$ and (**c**) overall average intensity in the propagation plane xz. The maximum rotation Γ_0 is equal to 0, 15 and 45° from left to right, respectively. The input wave is RCP. Here $w_D = 5$ μm.

Supplementary Fig. 4 shows how power is distributed between the two components E_x and E_y when light is guided: $|E_x|^2$ and $|E_y|^2$ distributions in the plane xz essentially coincide. The overall intensity is computed as $\bar{n}/(2Z_0)\left(|E_x|^2 + |E_y|^2\right)$ with Z_0 the vacuum wave impedence, thus ignoring impedance variations for the two polarizations.

D. Dependence on the transverse size of the effective waveguide

Another important feature of the system is its dependence on the transverse extent of the orientation angle distribution. Both circular polarizations are shown in Supplementary Fig. 5. In agreement with theory, the smaller w_D the stronger is the repulsion of the defocused component from the perturbed region. Light spatial localization increases as w_D reduces, with intensity oscillations becoming slower in space as the θ distribution gets wider and wider. In line with Eqs. (S15-S16), light confinement undergoes the same trend as in standard waveguides based on total internal reflection.

E. Dependence on the input point

Finally, we studied light propagation as the longitudinal modulation $\sigma(z)$ was shifted, that is, as the phase Φ in $\sigma = \sin\left[\frac{2\pi\Delta n}{\lambda}(z - z_0) + \Phi\right]$ was modified. Supplementary Fig. 6 shows the FDTD results: as predicted (Eqs. (S17-S18)), when the phase is inverted (i.e., $\Phi = \pi$) the two circular polarizations exchange roles, with RCP waves going from trapping to anti-guiding and the opposite for LCP; when $\Phi = \pi/2$, the intensity evolution remains the same regardless the input ellipticity: this agrees with Supplementary Fig. 2 showing quasi-linear polarization at a quarter

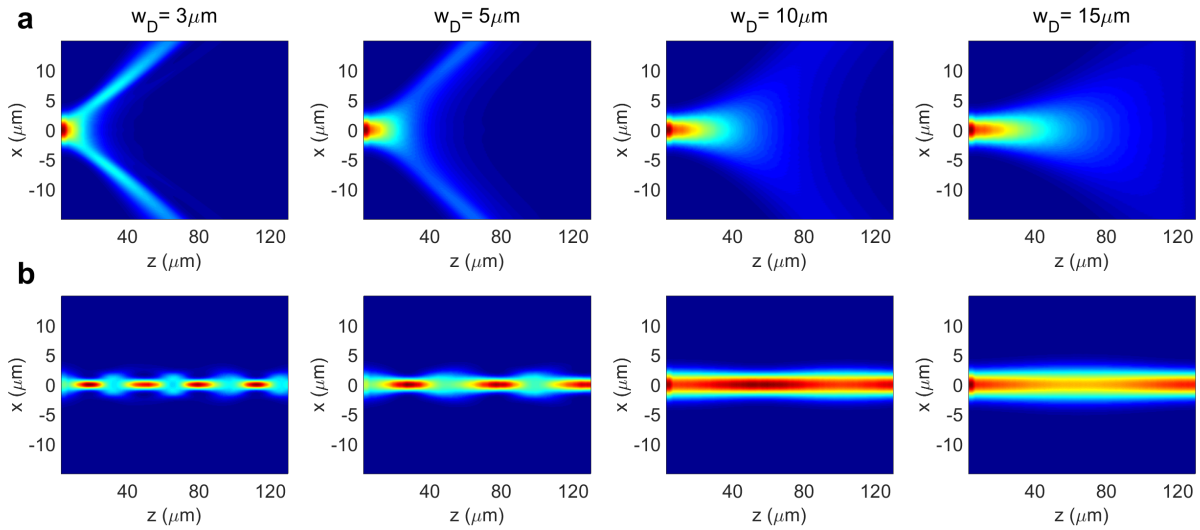

Supplementary Figure 5. Average intensity evolution in the propagation plane xz for (**a**) left- and (**b**) right-handed circularly polarized wavepackets. Here $\Gamma_0 = 45^\circ$ whereas the angular distribution width w_D is 3, 5, 10 and 15 μm from left to right, respectively.

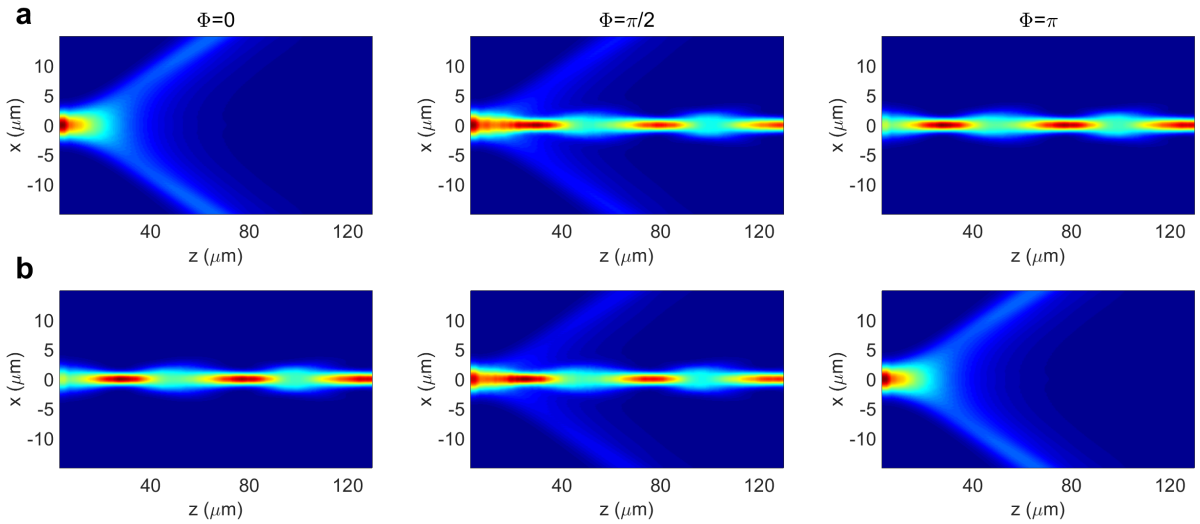

Supplementary Figure 6. Wavepacket evolution in xz for input LCP (**a**) and RCP (**b**) when the longitudinal modulation shift Φ is 0, $\pi/2$ and π, from left to right, respectively. Here $\Gamma_0 = 45^\circ$ and $w_D = 5$ μm.

period.

---

[1] The propagation constant remains wavelength dependent through the vacuum wavevector on the LHS of Eqs. (S15-S16).

[2] A. Alberucci, L. Marrucci, and G. Assanto, New Journal of Physics **15**, 083013 (2013).

[3] A. F. Oskooi, D. Roundy, M. Ibanescu, P. Bermel, J. D. Joannopoulos, and S. G. Johnson, Computer Physics Communications **181**, 687 (2010).

[4] This contribution is $O(\Lambda^2)$ and was neglected when deriving Eqs. (S7-S8): in the complete expression the term $\sum_{p>1}\left(\int \frac{\partial\beta_p^{(j)}}{\partial x}dz \int \frac{\partial\beta_{-p}^{(j)}}{\partial x}dz\right)$ $(j = e, o)$ appears within square brackets and brings in the role of all the fast scales on the slow scale.